Electronic Supplementary Material (ESI) for Journal of Materials Chemistry B.

Highly sensitive non-enzymatic electrochemical glucose sensor surpassing water oxidation interference

Neha Thakur, Debaprasad Mandal* and Tharamani C. Nagaiah,*

Department of Chemistry, Indian Institute of Technology Ropar Rupnagar, Punjab-140001, India

tharamani@iitrpr.ac.in, dmandal@iitrpr.ac.in

Table S1: Illustrating the amount taken during synthesis.

NiVP/Pi	$NiCl_2.6H_2O$ (g) (1.05 m mol)	NH_4VO_3 (g) (1.05 m mol)	Urea (g) (18.9 m mol)	NH_4F (g) (18.9 m mol)
NiV(1:2)P/Pi	0.250	0.245	1.134	0.699
NiV(1:1)P/Pi	0.250	0.123	1.134	0.699
NiV(2:1)P/Pi	0.498	0.123	1.134	0.699
NiV(3:1)P/Pi	0.748	0.123	1.134	0.699

Fabrication of flexible paper electrode: Flexible paper electrode was prepared by simple drop-casting method, in which NiVP/Pi catalyst slurry was drop coated onto Whatman filter paper (1.1 mm thickness) with an area of 0.12 cm^2 and the contact was made through the Cu wire using Ag-paste and sealed with Teflon tape and was dried at room temperature. NiVP/Pi catalyst coated Whatman filter paper serves as binder-free flexible working electrode for electrochemical measurement.

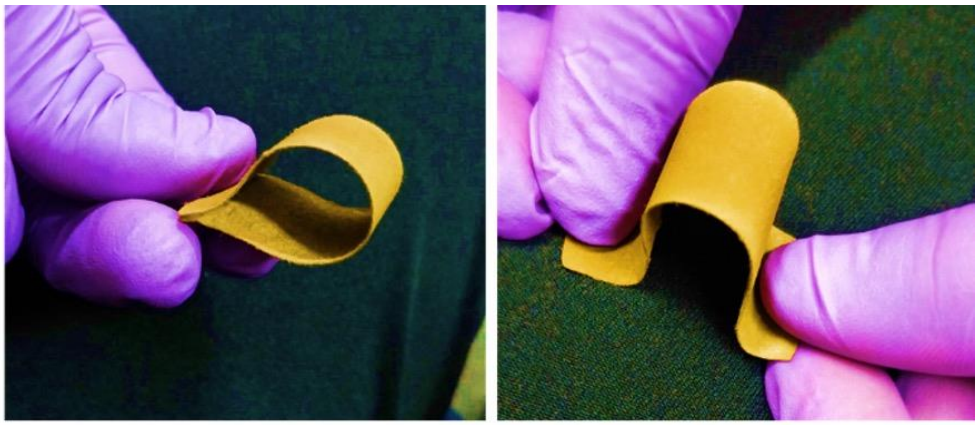

Scheme S1: Schematic representation of the flexible paper electrode.

Table S2: MP-AES results of NiVP/Pi catalysts.

NiVP/Pi	Feeding molar ratio of Ni:V	Actual molar ratio of Ni:V
NiV(1:2)P/Pi	1 : 2	1: 2.1
NiV(1:1)P/Pi	1 : 1	1.1 : 1
NiV(2:1)P/Pi	2 : 1	2.1 : 1
NiV(3:1)P/Pi	3 : 1	2.9 : 1

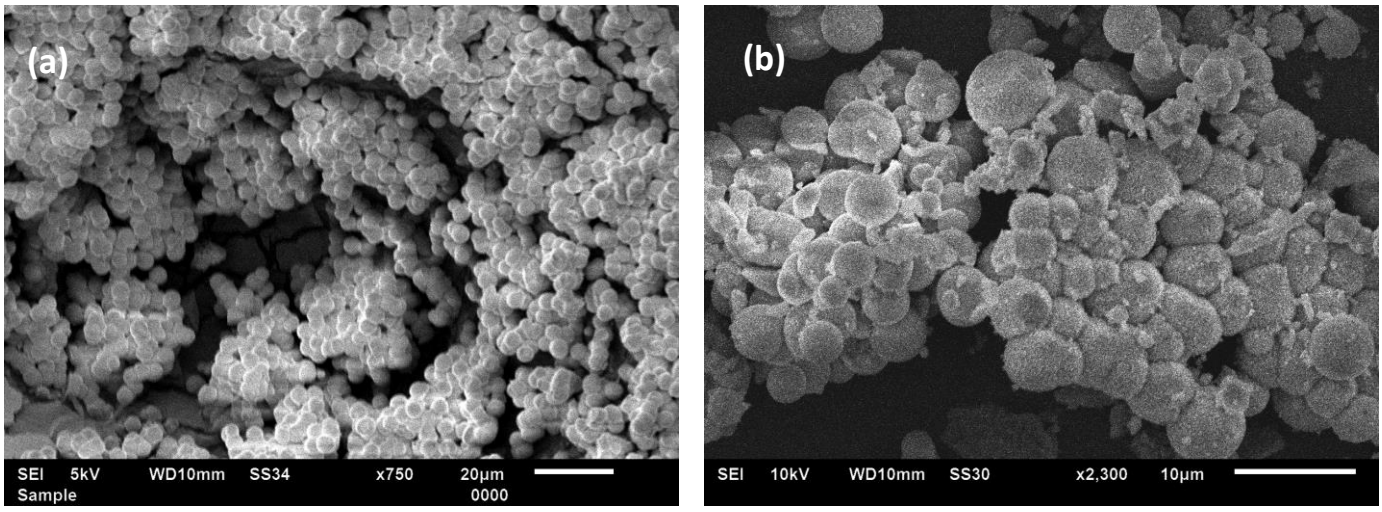

Figure S1. SEM image of (a) NiV(1:1)LDH and (b) NiV(1:1)P/Pi catalyst.

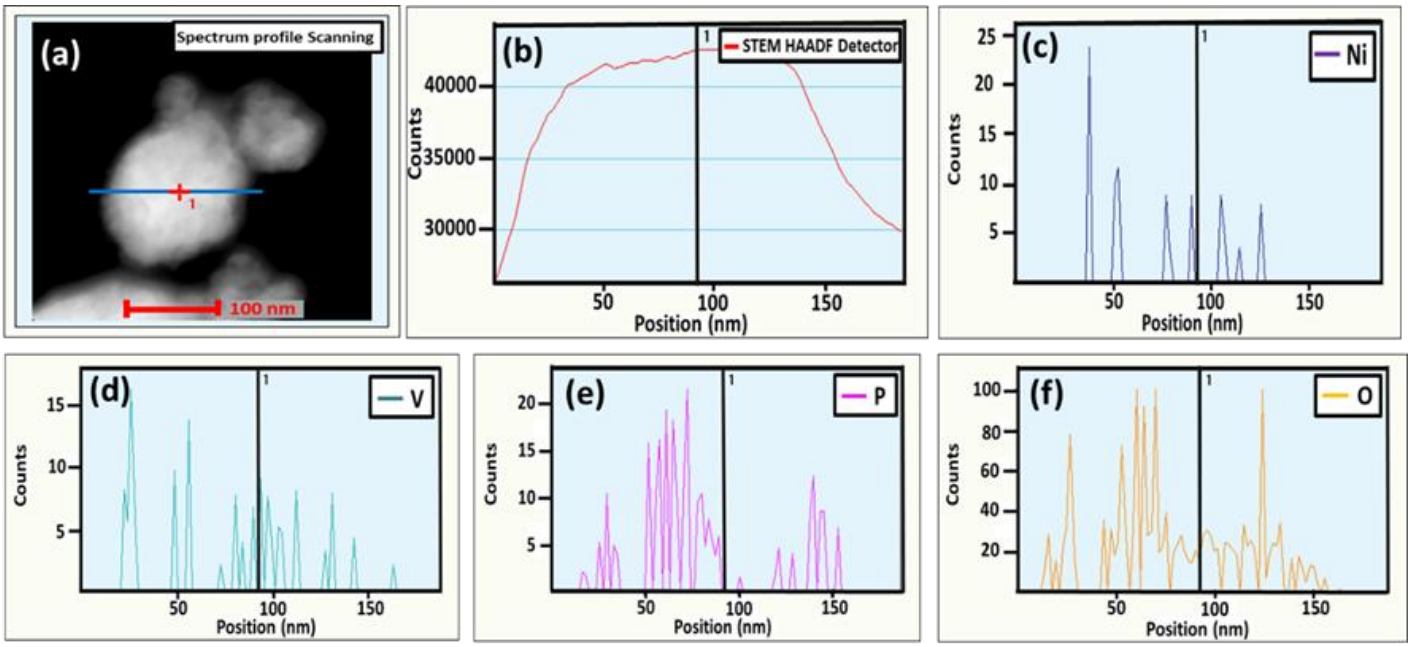

Figure S2. STEM line spectrum profile of NiV(2:1)P/Pi catalyst representing the distribution of Ni, V, P and O elements.

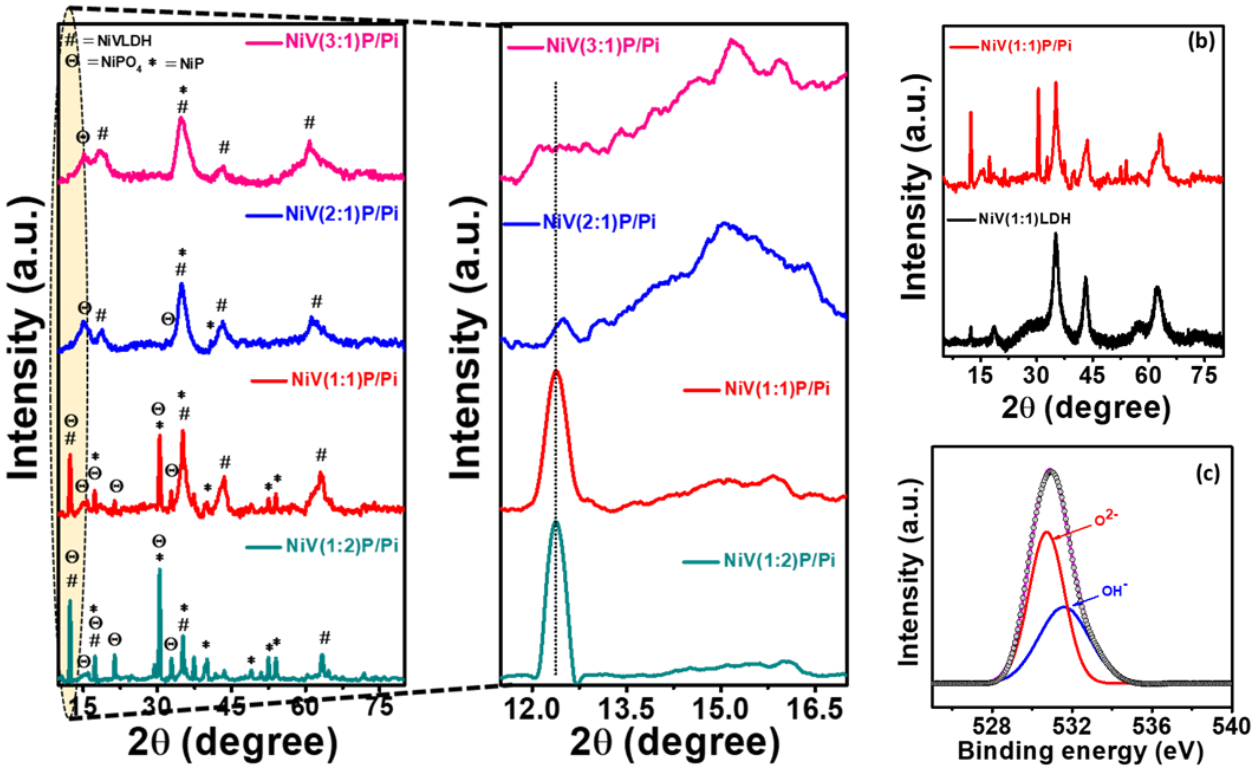

Figure S3. (a) and (b) XRD pattern of NiVP/Pi catalysts, (c) O 1s XP spectra of NiV(2:1)P/Pi catalyst.

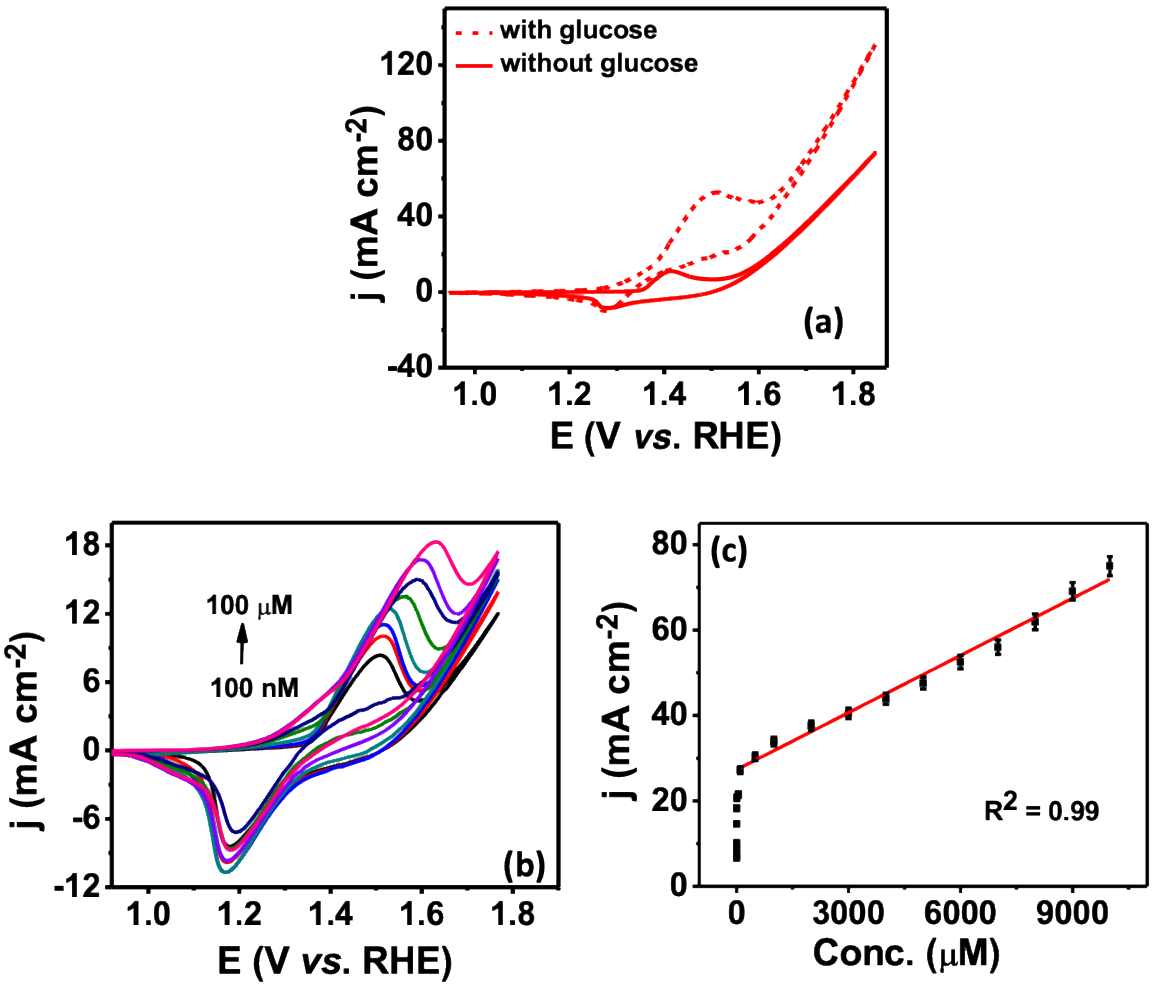

Figure S4. (a) Cyclic voltammograms comparison of NiV(1:1)P/Pi in 0.1 M NaOH electrolyte at a scan rate of 5 mV s^{-1}, (b) CV response with Ni foam alone in 0.1 M NaOH electrolyte containing various conc. of glucose at a scan rate of 5 mV s^{-1}, (c) Plot of current density versus concentration of glucose for NiV(1:1)P/Pi catalyst extracted from chronoamperometric study (Fig. 2f), CE: Pt wire, RE: double junction Ag/AgCl/3 M KCl.

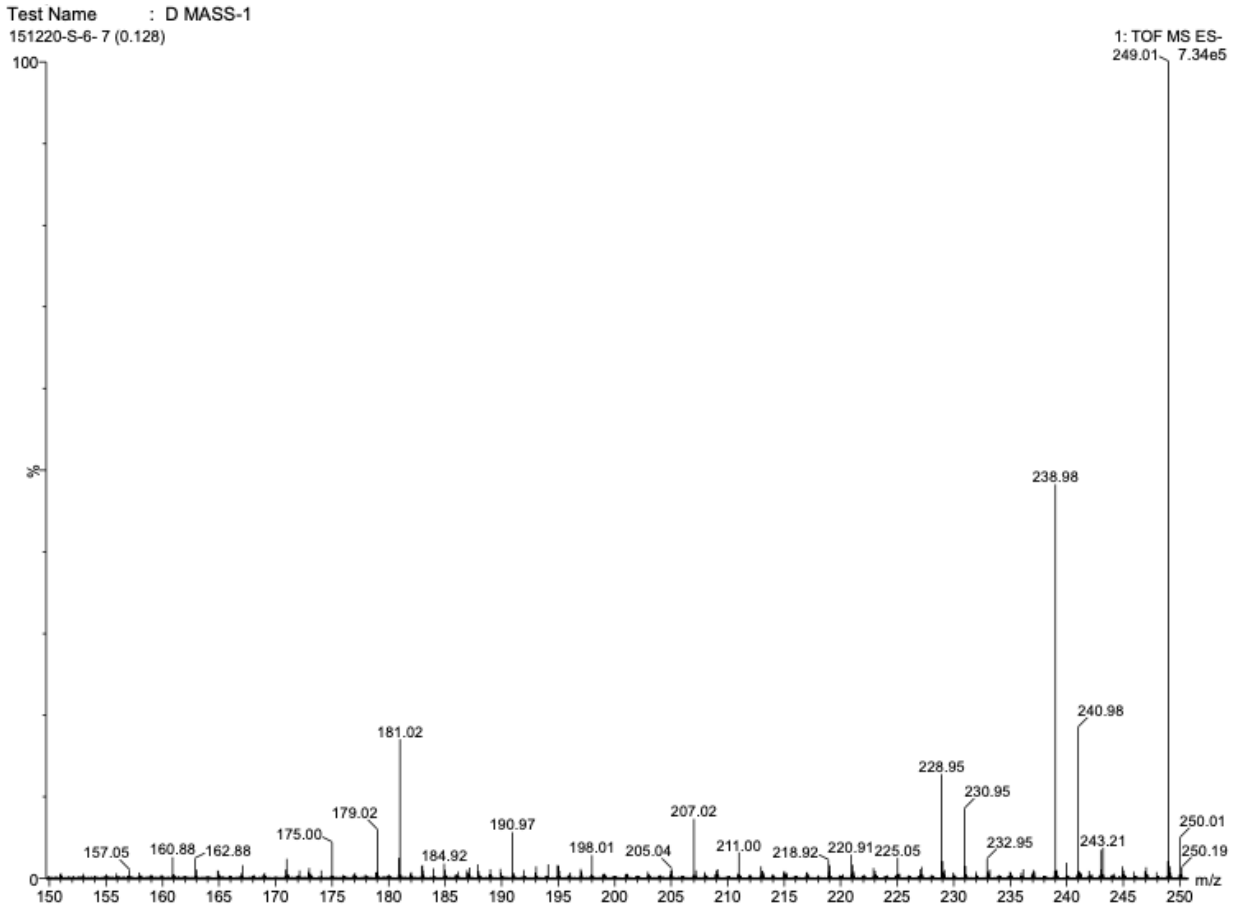

Figure S5. HRMS data of glucose oxidation.

	Glucose	Gluconolactone	Gluconic acid	Glucaric acid
Parent Peak	180	178.14	196	210.14
[M+1H]	181	179		211
Adduct with (Na^+-2H)	202.97	198.01	218.92	230.95
Adduct with ($2Na^+$-3H)	-	220.9	238.98	253
Adduct with (Na^++H2O-2H)		-	-	249.01

HR-MS analysis: To understand the product of the electrooxidation of glucose, the LC-MS measurement were performed using the electrolyte after the CV experiment with NiV(1:1)P/Pi catalyst in 0.1 M NaOH containing 200 µM of glucose. The results clearly illustrate the formation of oxidized products, describing the electro-oxidation of glucose.

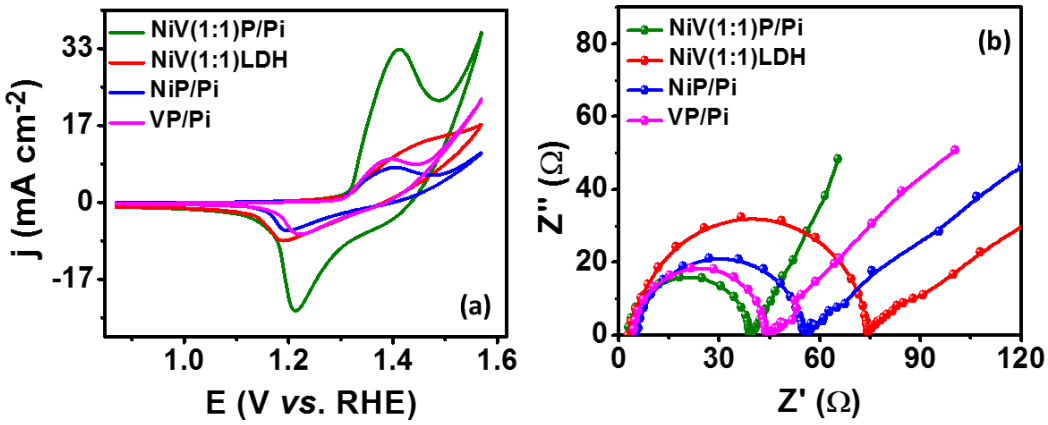

Figure S6. (a) Cyclic voltammograms and (b) EIS result for various catalysts in 0.1 M NaOH electrolyte containing 1 mM glucose at a scan rate of 5 mV s^{-1}, CE: Pt wire, RE: double junction Ag/AgCl/3 M KCl.

Electrochemical surface area (ECSA)

Electrochemically active surface area of the catalyst was determined by calculating the double-layer pseudo-capacitance (C_{dl}) in the non-faradaic region in 0.1 M NaOH with an analyte solution. CV was performed in non-faradic region/double-layer region in potential range from 0.02 V to 0.15 V *vs.* Ag/AgCl/3 M KCl double junction at various scan rates (50 to 600 mV s^{-1}). The slope of the plot between averaged current density of anodic and cathodic current $(I_a+I_c)/2$ (where, 'a' denotes anodic current and 'c' is for cathodic current) *vs*. the scan rate at 0.085 V *vs.* Ag/AgCl/3 M KCl gives pseudo-capacitance. C_{dl} was dividing with the specific capacitance (C_s) of the flat standard surface (20-60 µF cm^{-2}), which is considered to be 40 µF cm^{-2}, gives electrochemical surface area (ECSA). The roughness of the surface was calculated by dividing the obtained ECSA with the geometrical surface area.

ECSA calculation:[1]

ECSA = C_{dl} / C_s

Table S3: Electrochemical surface area (ECSA) analysis.

S.No.	Catalyst	C_{dl} (µF) at 0.955 V *vs.* RHE	ECSA (cm^2)
1.	NiV(1:1)P/Pi	222	6.55
2.	NiV(1:1)LDH	220.8	5.52
3.	NiP/Pi	145.2	3.63
4.	VP/Pi	194.4	4.86

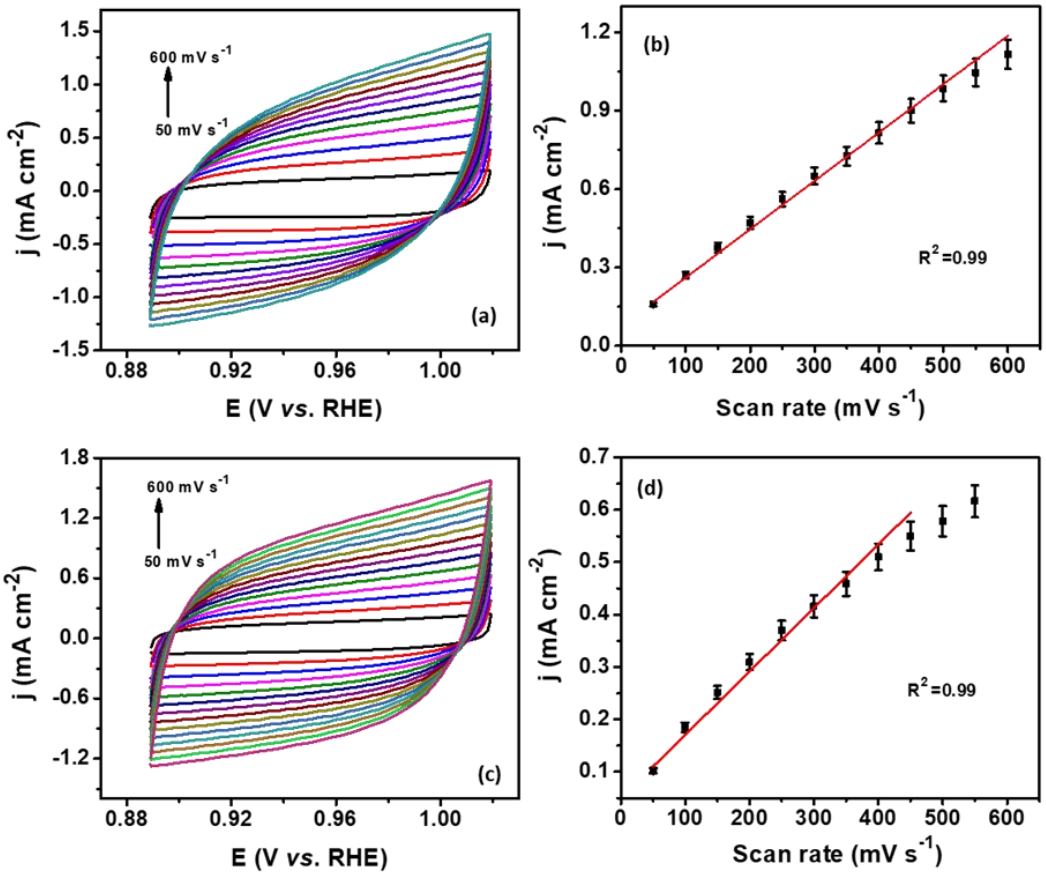

Figure S7. Cyclic voltammograms of (a) NiV(1:1)P/Pi and (c) NiP/Pi at varying scan rates in the non-faradic potential region and (b & d) corresponding average current density respectively *vs.* scan rate at varying scan rates ranging from 50 to 600 mV s^{-1}; CE: Pt wire, RE: double junction Ag/AgCl/3 M KCl.

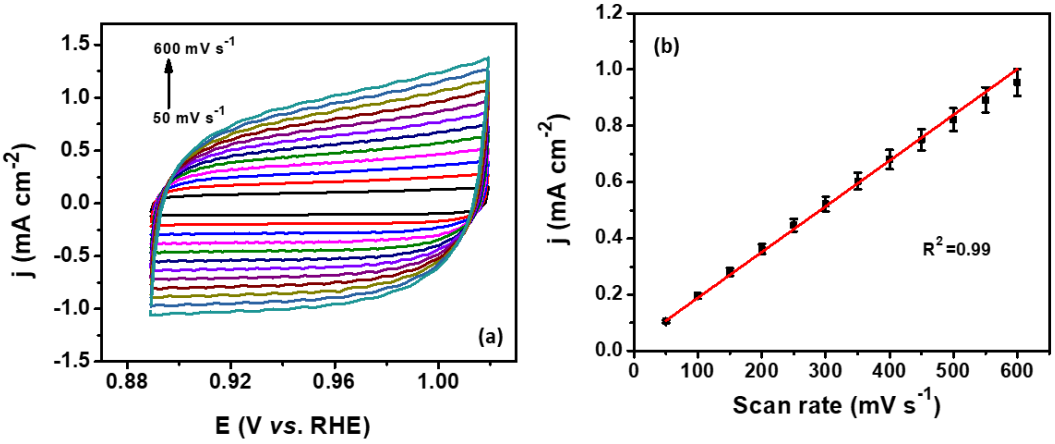

Figure S8. Cyclic voltammograms of (a) NiV(1:1)LDH at varying scan rates in the non-faradic potential region and (b) corresponding average current density respectively *vs.* scan rate at varying scan rates ranging from 50 to 600 mV s^{-1}; CE: Pt wire, RE: double junction Ag/AgCl/3 M KCl.

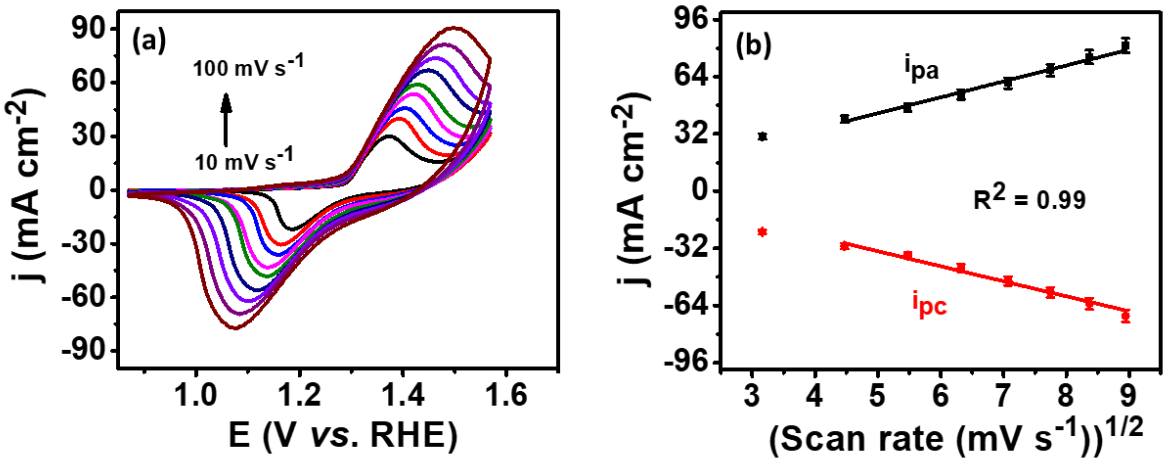

Figure S9. (a) Cyclic voltammograms of NiV(1:1)P/Pi catalyst at various scan rates, and (b) corresponding average current density *vs.* scan rate in 0.1 M NaOH electrolyte containing 1 mM glucose CE: Pt wire, RE: double junction Ag/AgCl/3 M KCl.

The effect of scan rate (scan rates ranged from 10 to 100 mV s^{-1}) of the NiV(1:1)P/Pi material on the electrochemical response at 1 mM glucose was investigated by CV (Fig. S9). With increasing scan rate, the oxidation and reduction currents (I_{pa} and I_{pc}) increased, and simultaneously the anodic peak potential shifted slightly positively and negatively for the cathodic peak potential. The plot between anodic peak current (I_{pa}) and the cathodic peak current (I_{pc}) *vs*. the square root of the scan rate showed a linear relationship inferring that the electrooxidation of glucose by NiV(1:1)P/Pi is a typical diffusion-controlled process.

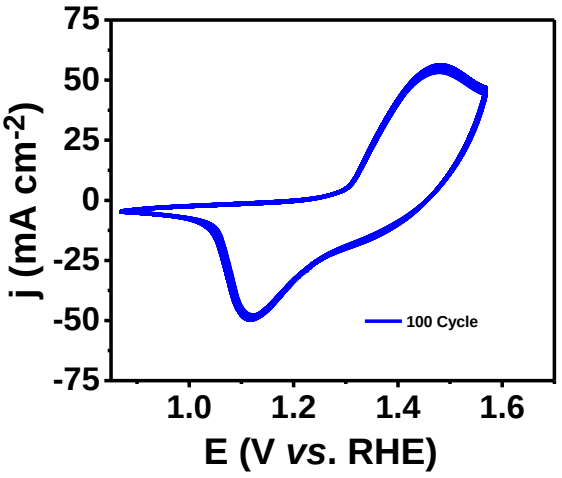

Figure S10. Cyclic voltammograms of NiV(1:1)P/Pi catalyst in 0.1 M NaOH electrolyte containing 1 mM glucose for 100 cycles at a scan rate of 50 mV s^{-1}, CE: Pt wire, RE: double junction Ag/AgCl/3 M KCl.

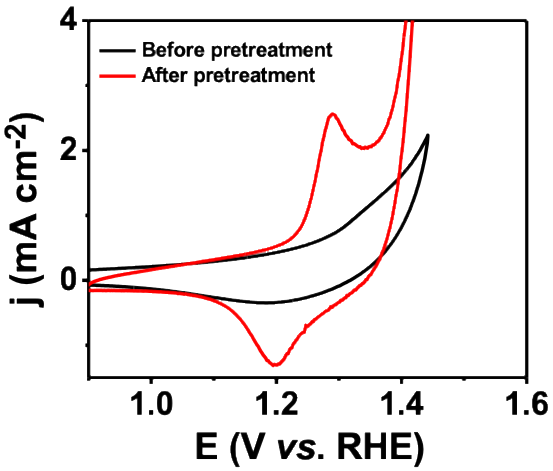

Figure S11. Cyclic voltammograms of NiV(1:1)P/Pi over paper electrode before and after pretreatment in 0.1 M PBS electrolyte (pH =7.4)); CE: Pt wire, RE: double junction Ag/AgCl/3 M KCl.

In the present work, for detection in the physiological pH (0.1 M PBS) the experiments were performed by applying pre-conditioning potential of −2.0 V for 30 s, on the NiV(1:1)P/Pi electrode followed by glucose addition for sensing. At this potential, protons were reduced on the electrode surface, which produces a localized alkaline environment on the electrode surface for glucose detection.[2-4] The obtained cyclic voltammogram after preconditioning at −2.0 V exhibited well-defined redox behaviour, corresponding to the Ni(II)/(III) as shown in the Fig. S12A. With sequential addition of glucose, peak currents increases (Fig. 3b), suggesting that NiV(1:1)P/Pi catalyst can effectively catalyze the electrochemical glucose oxidation even at physiological pH. The obtained oxidation current was found to be in linear correlation with the glucose concentration (inset) with a superior sensitivity of 1670 μA mM^{-1} cm^{-2}.

Furthermore, in order to validate the applicability of the proposed sensor in practical applications for the detection of glucose, NiV(1:1)P/Pi catalyst was analyzed in real sample using human blood serum via standard addition method. Serum sample was injected in 0.1 M NaOH electrolyte and known amounts of glucose in the test solution was added. The obtained results are tabulated in Table S4 (SI). The recovery of the spiked sample ranges from 99 to 113, which determine the applicability of the proposed sensor for real time application as well.

Table S4. Human serum sample analysis with NiV(1:1)P/Pi modified electrode.

Sample	**Actual Conc.**	**Conc. (Added)**	**Conc. (found)**	**Recovery (%)**
1.	100 μM	100 μM	198 μM	99
2.	100 μM	200 μM	339 μM	113

Figure S12A. Images displaying change of pH by applying -2 V in 0.1 M PBS (pH 7.4) solution containing 5 µL of 5% phenolphthalein (in ethanol) in the electrochemical cell; CE: Pt wire, RE: double junction Ag/AgCl/3 M KCl.

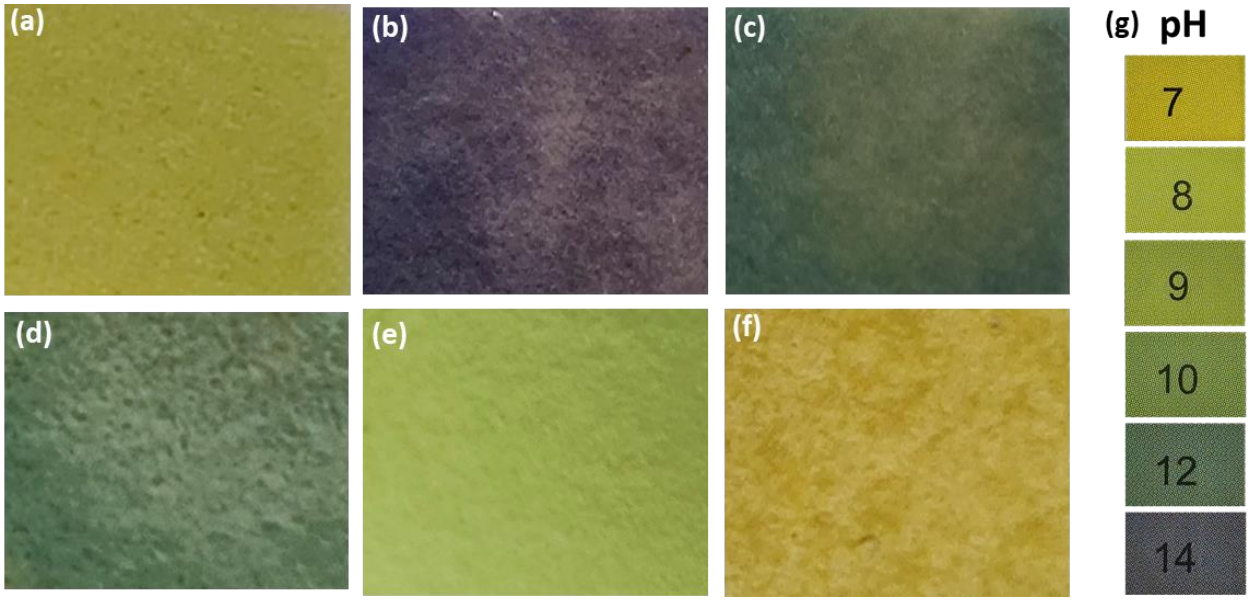

Figure S12B. Color change on pH test strips of solution samples under static condition at different time, (a) before pretreated, (b-f) after pretreated for 0.5 min, 1 min, 2 min, 5 min, 7 min, (g) standard color change of the pH test strips.

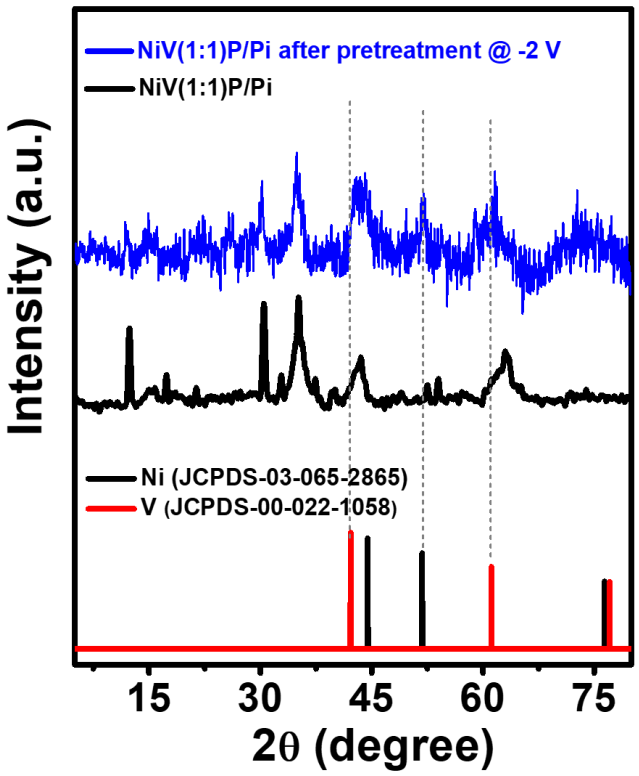

Figure S12C. XRD pattern of NiV(1:1)P/Pi catalyst after pretreatment along with standard profiles.

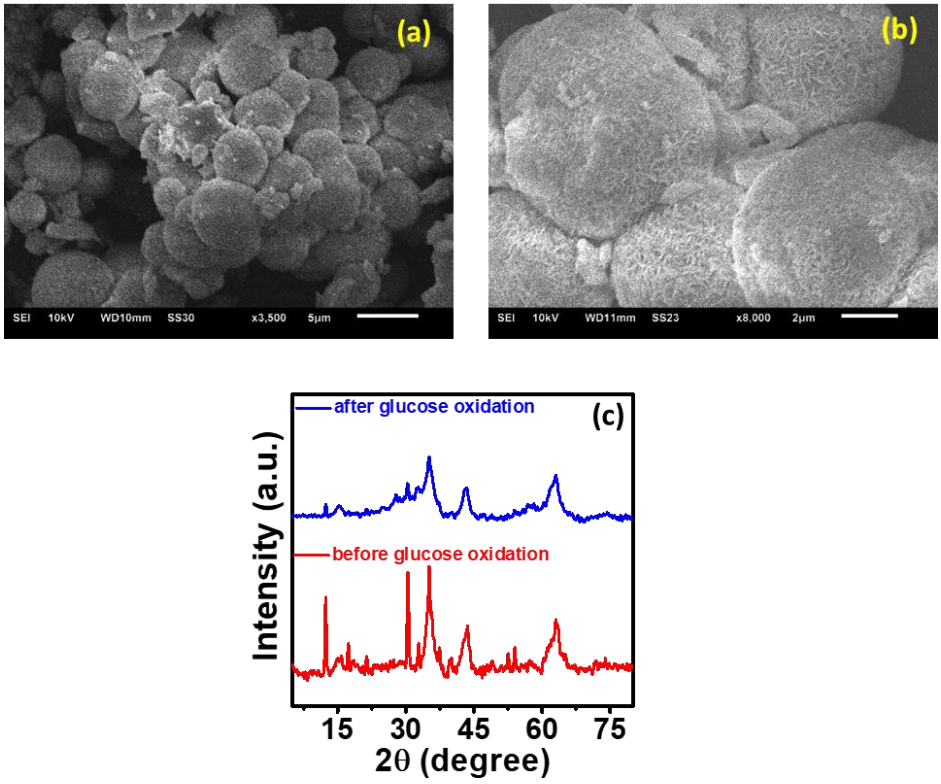

Figure S13A. (a-b) SEM images and (c) XRD pattern of NiV(1:1)P/Pi before and after glucose oxidation.

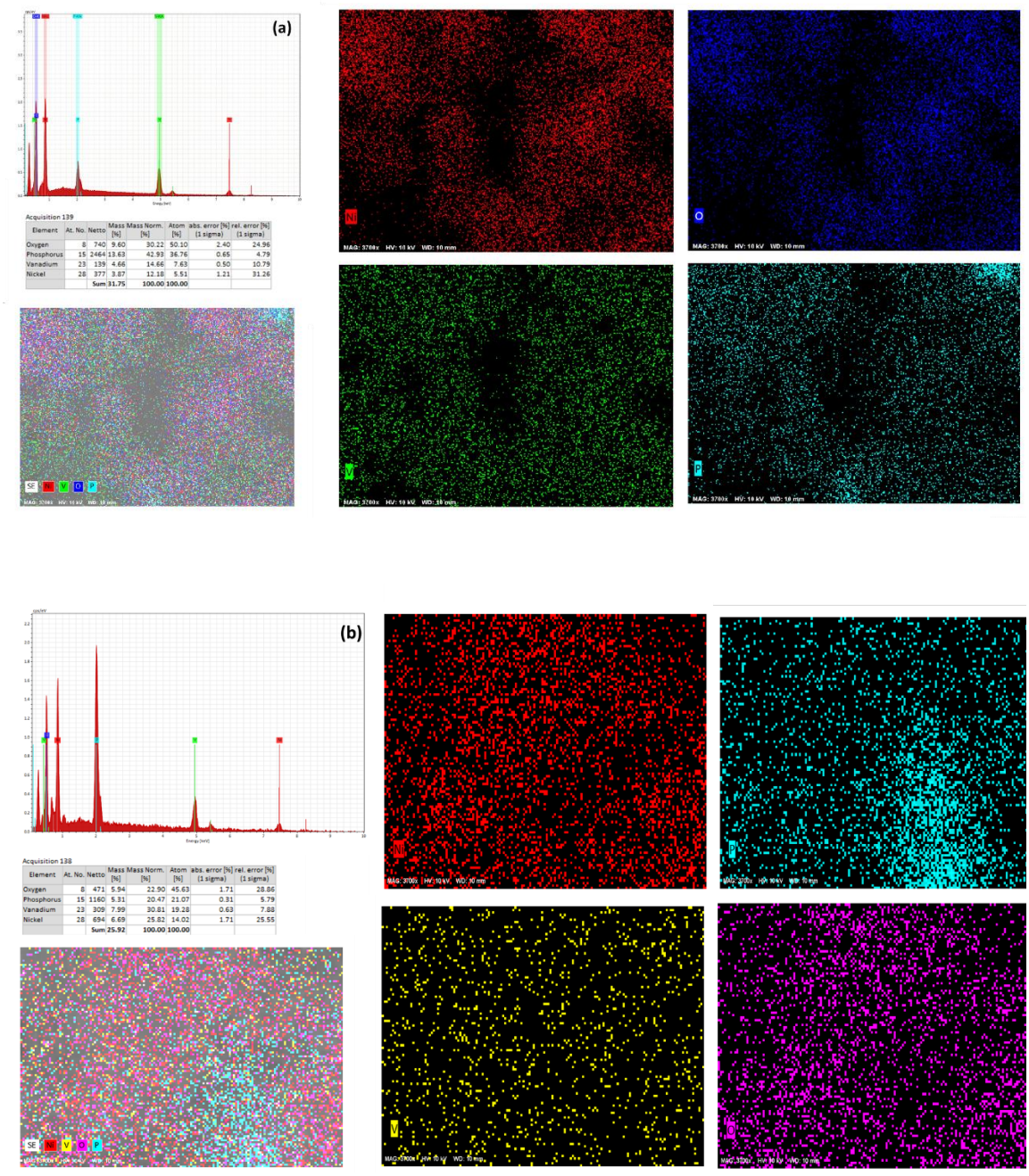

Figure S13B. EDS dot mapping of NiV(1:1)P/Pi catalyst (a) before and (b) after glucose oxidation.

Table S5. Comparison of analytical performance of glucose sensor with various modified electrodes reported previously.

Electrode	Linear range	Lowest detection limit (μM)	Sensitivity ($\mu A\ mM^{-1}\ cm^{-2}$)	Ref.
$W_{18}O_{49}$ electrode.		0.02	167	4
$Ni_{60}Nb_{40}$ nanoglass	100 μM-2 mM	100 nM	20000	5
Cu_2O MSs/S-MWCNTs	4.95 μM-7 mM	1.46	581.89	6
LIO-Ni electrode	5 μM-1.1mM	3.31	5222	7
CoFe-PBA/Co-ZIF/NF	1.4 μM-1.5 mM	0.02	5270	8
Ni_4Fe-LDH & Ni_4Fe/rGO_5	0−4 mM		20.43 &176.8	9
CuO nanostructures	5 μM-0.225 mM	0.41	3072	10
Ni_3N NS/Ti	0.2 μM-1.5 mM	0.06	7688	11
CuO PNBs	0.1 μM-2 mM	0.06	1876.52	12
M-BDC MOFs	10 μM -0.8 mM	6.68	635.9	13
Ag–PANI/rGO	0.1 μM-0.05 mM	0.79	2.7664	14
Ni/Co UMOFNs	0.1 μM-1.4 mM	0.047	2086.7	15
HMCA/NF	5 μM-2.5 mM	0.43	2.194	16
Copper-G-COOH	0.1 μM-5.48 mM	.00796	1142	17
SWCNTs/Cu_2O/ZnO NRs SWCNTs/Cu_2O/ZnO NRs/graphene	600 μM-11.1 mM (0−5.556) mM & (5.556−11.111) mM		289.8 466.1 & 203.1	18
GS@ZIF-67 hybrids	1 μM-0.8055 mM	0.36	1521.1	19
$Co_{0.33}Ni_{0.67}$-HLDH/GCE	10 μM-2.0 mM	3.1	242.9	20
ND-Gr-NH	5 μM-2 mM	0.1	15431.2	21
E-NiCo-BTC/GCE	0.001-1.78 &5.03 mM	0.187	1789 & 1436	22
Ag@ZIF-67	2 μM-1 mM	0.66	0.379	23
Ni-MOF/Ni/NiO/C	4 μM-5.664 mM	0.8	367.45	24
Ni_2P/G	5 μM-1.4 mM	0.44	7234	25
No−Co phosphate	2 μM-4.470 mM	0.4	302.99	26
Cu−Co/rGO/PGE	1 μM-4 mM	0.15	240	27
$Ni(OH)_2$@3DPN	0.46 μM-2.1 mM	0.46	2761.6	28
VS_2/Nf/GCE	0.5 μM-3 mM	0.211	41.96 $\mu A\ mM^{-1}$	29
NiS/S-g-C_3N_4	0.1 μM-2.1 mM	1.5	80	30
NiVP/Pi	**100 nM - 1 μM 100 μM - 10 mM**	**3.7 nM**	**6040 $\mu A\ \mu M^{-1}\ cm^{-2}$ 4460 $\mu A\ \mu M^{-1}\ cm^{-2}$**	**This Work**

References

1. S. Lupu, C. Lete, M. Marin, N. Totir and P. C. Balaure, *Electrochim. Acta*, 2009, **54**, 1932-1938.
2. X. Zhu, Y. Ju, J. Chen, D. Liu and H. Liu, *ACS Sens.*, 2018, **3**, 1135-1141.
3. X. Zhu, S. Yuan, Y. Ju, J. Yang, C. Zhao and H. Liu, *Anal. Chem.*, 2019, **91**, 10764-10771.
4. L. Sinha, H. Lee, Y. Ohshita and P. M. Shirage, *ACS Biomater. Sci. Eng.*, 2020, **6**, 1909-1919.
5. S. Bag, A. Baksi, S. H. Nandam, D. Wang, X. Ye, J. Ghosh, T. Pradeep and H. Hahn, *ACS nano*, 2020, **14**, 5543-5552.
6. M. Waqas, L. Wu, H. Tang, C. Liu, Y. Fan, Z. Jiang, X. Wang, J. Zhong and W. Chen, *ACS Appl. Nano Mater.*, 2020, **3**, 4788-4798.
7. S. Sedaghat, C. R. Piepenburg, A. Zareei, Z. Qi, S. Peana, H. Wang and R. Rahimi, *ACS Appl. Nano Mater.*, 2020, **3**, 5260-5270.
8. C. Chen, D. Xiong, M. Gu, C. Lu, F.-Y. Yi and X. Ma, *ACS Appl. Mater. Interfaces*, 2020, **12**, 35365-35374.
9. S. Moolayadukkam, S. Thomas, R. C. Sahoo, C. H. Lee, S. U. Lee and H. R. Matte, *ACS Appl. Mater. Interfaces*, 2020, **12**, 6193-6204.
10. P. Chakraborty, S. Dhar, N. Deka, K. Debnath and S. P. Mondal, *Sens. Actuators B Chem.*, 2020, **302**, 127134.
11. F. Xie, T. Liu, L. Xie, X. Sun and Y. Luo, *Sens. Actuators B Chem.*, 2018, **255**, 2794-2799.
12. Y.-Y. Li, P. Kang, H.-Q. Huang, Z.-G. Liu, G. Li, Z. Guo and X.-J. Huang, *Sens. Actuators B Chem.*, 2020, **307**, 127639.
13. G. Gumilar, Y. V. Kaneti, J. Henzie, S. Chatterjee, J. Na, B. Yuliarto, N. Nugraha, A. Patah, A. Bhaumik and Y. Yamauchi, *Chem. Sci.*, 2020, **11**, 3644-3655.
14. M. A. Deshmukh, B.-C. Kang and T.-J. Ha, *J. Mater. Chem.*, 2020, **8**, 5112-5123.
15. H. Zou, D. Tian, C. Lv, S. Wu, G. Lu, Y. Guo, Y. Liu, Y. Yu and K. Ding, *J. Mater. Chem. B*, 2020, **8**, 1008-1016.
16. N. I. Chandrasekaran and M. Matheswaran, *ACS Omega*, 2020, **5**, 23502-23509.
17. S. Wu, Y. Zhang, L. Liu and W. Fan, *Mater. Lett.*, 2020, **276**, 128253.
18. H.-C. Chen, W.-R. Su and Y.-C. Yeh, *ACS Appl. Mater. Interfaces*, 2020, **12**, 32905-32914.
19. X. Chen, D. Liu, G. Cao, Y. Tang and C. Wu, *ACS Appl. Mater. Interfaces*, 2019, **11**, 9374-9384.
20. X. Kong, B. Xia, Y. Xiao, H. Chen, H. Li, W. Chen, P. Wu, Y. Shen, J. Wu and S. Li, *ACS Appl. Nano Mater.*, 2019, **2**, 6387-6396.
21. B.-R. Huang, D. Kathiravan, C.-W. Wu and W.-L. Yang, *ACS Appl. Bio Mater.*, 2020, **3**, 5966-5973.
22. M. Ezzati, S. Shahrokhian and H. Hosseini, *ACS Sustain. Chem. Eng.*, 2020.
23. Q. Wa, W. Xiong, R. Zhao, Z. He, Y. Chen and X. Wang, *ACS Appl. Nano Mater.*, 2019, **2**, 4427-4434.
24. Y. Shu, Y. Yan, J. Chen, Q. Xu, H. Pang and X. Hu, *ACS Appl. Mater. Interfaces*, 2017, **9**, 22342-22349.
25. Y. Zhang, J. Xu, J. Xia, F. Zhang and Z. Wang, *ACS Appl. Mater. Interfaces*, 2018, **10**, 39151-39160.
26. Y. Shu, B. Li, J. Chen, Q. Xu, H. Pang and X. Hu, *ACS Appl. Mater. Interfaces*, 2018, **10**, 2360-2367.
27. K. Justice Babu, S. Sheet, Y. S. Lee and G. Gnana kumar, *ACS Sustain. Chem. Eng.*, 2018, **6**, 1909-1918.
28. W. Mao, H. He, P. Sun, Z. Ye and J. Huang, *ACS Appl. Mater. Interfaces*, 2018, **10**, 15088-15095.
29. A. Sarkar, A. B. Ghosh, N. Saha, G. R. Bhadu and B. Adhikary, *ACS Appl. Nano Mater.*, 2018, **1**, 1339-1347.
30. S. Vinoth, P. M. Rajaitha, A. Venkadesh, K. S. Shalini Devi, S. Radhakrishnan and A. Pandikumar, *Nanoscale Adv.*, 2020, **2**, 4242-4250.